Temporal Specificity in the Cortical Plasticity of Visual Space Representation

Yu-Xi Fu,* Kaj Djupsund,* Hongfeng Gao,* Benjamin Hayden, Kai Shen, Yang Dan†

The circuitry and function of mammalian visual cortex are shaped by patterns of visual stimuli, a plasticity likely mediated by synaptic modifications. In the adult cat, asynchronous visual stimuli in two adjacent retinal regions controlled the relative spike timing of two groups of cortical neurons with high precision. This asynchronous pairing induced rapid modifications of intracortical connections and shifts in receptive fields. These changes depended on the temporal order and interval between visual stimuli in a manner consistent with spike timing–dependent synaptic plasticity. Parallel to the cortical modifications found in the cat, such asynchronous visual stimuli also induced shifts in human spatial perception.

Persistent synaptic modification can be induced by repetitive pairing of pre- and postsynaptic spikes, and the direction and magnitude of the modification depend on the relative spike timing (*1–6*). Presynaptic spiking within 10s of milliseconds before postsynaptic spiking induces synaptic potentiation, whereas the reverse order results in synaptic depression. Spike timing–dependent plasticity has been widely observed at excitatory synapses in vitro, and its functional significance has been discussed in a variety of neuronal circuits (*7–10*). However, whether and how this mechanism operates in vivo in response to sensory stimuli is only beginning to be examined experimentally (*11–13*). In the primary visual cortex, timing of visual stimuli can directly affect timing of neuronal spiking and thus, may play a role in activity-dependent cortical plasticity.

A simple working hypothesis of how relative timing of visual stimuli can affect cortical representation of visual space is illustrated in Fig. 1. Asynchronous stimuli in retinal regions *A* and *B* may evoke asynchronous spiking in two groups of cortical neurons, *a* and *b* (Fig. 1, A and B). According to spike timing–dependent synaptic plasticity, *A*→*B* stimulation may strengthen *a*→*b* connections and weaken *b*→*a* connections (Fig. 1C, left). Because intracortical connections contribute significantly to shaping the cortical receptive fields (*14*), the synaptic modifications induced by *A*→*B* stimuli may cause the receptive fields of both groups to shift toward *A* (*15*) (Fig. 1D, left). In a typical population-decoding scheme, the perceived stimulus location is determined by the spatial profile of population neuronal response (*16*). The leftward shift (toward *A*) of receptive fields should cause a rightward shift in the response profile, hence a rightward shift in perception (Fig. 1E, left). By symmetry, *B*→*A* stimuli that activate group *b* before *a* should cause the opposite changes at all levels (Fig. 1, right column).

Asynchronous Visual Conditioning

Receptive fields of primary visual cortical neurons recorded in anesthetized adult cats were mapped with strips of drifting gratings (Fig. 2A) (*17*). During visual conditioning, random spatial patterns were flashed asynchronously in two adjacent retinal regions (*A* and *B*, with receptive field of the recorded neuron in *B*) (Fig. 2B) to manipulate the relative spike timing of two groups of cortical neurons (*a* and *b*). In order for these stimuli to be effective in cortical modification, the precision of spike timing in the responses must be commensurate with the temporal requirement of spike timing–dependent synaptic plasticity on the order of 10s of milliseconds. We measured the spike timing precision by comparing the responses of each neuron to *A*→*B* and *B*→*A* stimuli. Spiking of a group *b* neuron during *A*→*B* stimuli (*A*/*B* interval: 8.3 ms) lagged behind its spiking during *B*→*A* stimuli by ~8 ms, indicating time-locking of the spikes to the flashed stimuli (Fig. 2C). The precision of spike timing is also reflected in the cross-correlation between the responses to *A*→*B* and *B*→*A* stimuli (Fig. 2D), which exhibited a distinct peak at ~8 ms, corresponding to the *A*/*B* interval. Such correspondence was also found in other experiments in which the *A*/*B* intervals ranged from 0 to 66.7 ms. The mean width at half height of the peak, which reflects spike timing precision, was 26 ± 15 ms (SD) for the 145 neurons examined (Fig. 2E). With such precision, *A*/*B* interval in the conditioning stimuli can effectively determine the relative spike timing between neuronal groups *a* and *b*.

Excitatory Intracortical Connections

To monitor intracortical synaptic modification, we applied cross-correlation analysis of simultaneously recorded cortical cell pairs (*18–23*). First, we analyzed the relationship between synaptic modifications and changes in intracortical cross-correlation using the model circuit depicted in Fig. 1A (*17*). As a result of spike timing–dependent synaptic plasticity, repetitive *A*→*B* conditioning potentiated *a*→*b* connections and depressed *b*→*a* connections, whereas *B*→*A* conditioning induced the opposite changes. Accompanying these synaptic modifications, two types of changes were observed in the cross-correlation between the spike trains of model neurons. First, for intragroup cross-correlation [b_i, b_j], conditioning induced changes

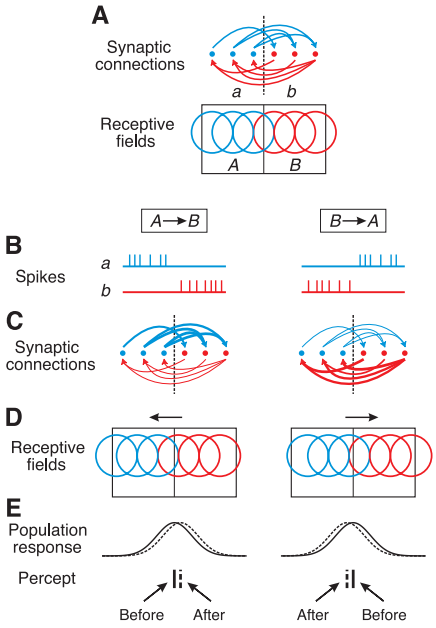

Fig. 1. A hypothetical scheme in which stimulus timing affects cortical modification. (**A**) Intracortical excitatory connections between two groups of neurons, *a* and *b*, whose receptive fields fall in *A* and *B*, respectively. Blue, group *a*; red, group *b*. Arrows indicate directions of axonal projections. Only a subset of connections between *a* and *b* are shown; connections within each group are omitted. (**B**) Relative spike timing of groups *a* and *b* in response to *A*→*B* and *B*→*A* stimuli. (**C**) Strength of connections between *a* and *b* (represented by line thickness) after conditioning, obtained from a simulation with 500 pairs of *A*→*B* (left) or *B*→*A* (right) conditioning (*17*). (**D**) Receptive fields after conditioning. Arrows indicate directions of shifts. (**E**) Spatial profiles of the population responses evoked by a test stimulus (vertical line) at *A*/*B* border before (solid curve) and after (dashed) conditioning.

Division of Neurobiology, Department of Molecular and Cell Biology, University of California, Berkeley, CA 94720, USA.

*These authors contributed equally to the work.
†To whom correspondence should be addressed. E-mail: ydan@uclink4.berkeley.edu

in correlation strength (measured by the area under the peak, Fig. 3A), reflecting modifications of the common inputs from group *a* neurons to b_i and b_j (see Fig. 3A legend). Second, for intergroup cross-correlation [a_i, b_j], conditioning induced shifts in correlation asymmetry (*24*) (Fig. 3B), reflecting modifications of both *a*→*b* and *b*→*a* connections (see legends).

In the first set of conditioning experiments, we measured changes in correlation strength between intragroup cell pairs (defined as group *b*). Shuffle-subtracted, flank-normalized cross-correlograms (*17*) were computed from the responses to mapping stimuli (Fig. 2A) before and after conditioning (Fig. 2B). In both examples shown in Fig. 4A, 1200 pairs of *A*→*B* conditioning at 8.3-ms interval (~2 min) induced a marked increase in correlation strength (dashed line), indicating potentiation of *a*→*b* connections (Fig. 3A, left), whereas the same amount of *B*→*A* conditioning induced a decrease in correlation strength (Fig. 4A, dotted line), indicating depression of the connections (Fig. 3A, right). For the 138 cell pairs examined, 1200 pairs of conditioning at 8.3-ms interval (*A*→*B*) induced an increase of 29.8 ± 4.2% (SEM, $P < 10^{-5}$, *t* test), and conditioning at −8.3-ms interval (*B*→*A*) induced an 18.2 ± 3.1% reduction ($P < 10^{-5}$). We further measured the effect of conditioning at *A*/*B* intervals ranging from −66.7 to 66.7 ms and found significant changes only within ±50 ms (Fig. 4B). To examine the persistence of the change induced by 1200 pairs of *A*→*B* conditioning (at the 8.3-ms interval) we measured the cross-correlation continuously in the absence of further conditioning. The change in correlation strength was found to persist for up to 8 min (Fig. 4C).

In a parallel set of conditioning experiments, we measured shifts in the asymmetry of cross-correlation between group *a* and group *b* neurons. In both examples shown in Fig. 4D, the shuffle-subtracted cross-correlograms measured after *A*→*B* (dashed) and *B*→*A* (dotted) conditioning at an 8.3-ms interval were laterally displaced from each other. The rightward shift of the peak after *A*→*B* conditioning suggests strengthening of *a*→*b* connections or weakening of *b*→*a* connections (Fig. 3B, left), whereas the leftward shift after *B*→*A* conditioning suggests the opposite changes (Fig. 3B, right). Because the effect of *B*→*A* conditioning on correlation [a_i, b_j] is equivalent to the effect of *A*→*B* conditioning on correlation [b_j, a_i] and because for each pair the designation of *a* and *b* is arbitrary, the measured effects of *A*→*B* and *B*→*A* conditioning were combined (see Fig. 4E legend). For the 58 cell pairs examined, 1200 pairs of conditioning stimuli at an 8.3-ms interval induced a 4.9 ± 1.5% (SEM, $P < 0.01$, *t* test) shift in correlation asymmetry in the predicted direction. We further measured the shift as a function of *A*/*B* interval from 0 to 66.7 ms (Fig. 4E) and found the effect restricted to a window of ~50 ms. Thus, shifts in the intergroup correlation asymmetry also depend on the *A*/*B* interval in a manner consistent with spike timing–dependent synaptic modification. In addition, we examined the persistence of the shift induced by 1200 pairs of conditioning stimuli (at an 8.3-ms interval) and found the effect to last for several minutes (Fig. 4F). This is similar to the persistence of conditioning-induced change in intragroup correlation strength (Fig. 4C), consistent with the idea that both types of changes in cross-correlation reflect the same set of intracortical synaptic modifications.

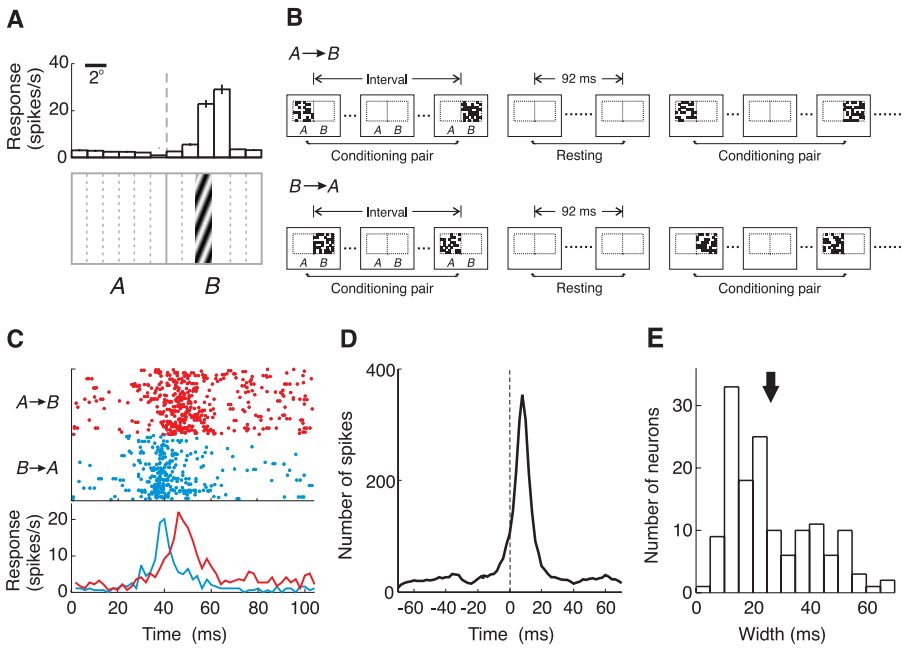

Fig. 2. Spike timing of cortical neurons in response to asynchronous conditioning stimuli. (**A**) Receptive field of a neuron (upper panel) and the mapping stimuli (lower panel). Error bars, ±SEM. Solid lines in lower panel delineate regions *A* and *B*; dotted lines indicate strip positions. (**B**) Two types of conditioning stimuli, *A*→*B* and *B*→*A*. The spatial patterns were either random checkerboards (8 × 8 pixels/region, in experiments shown in Fig. 4) or random bars at preferred orientation of the cell (16 bars/region, in experiments shown in Fig. 5) at 100% contrast. Size: 3.3 × 1.8° to 12.4 × 11.5°/region. In each conditioning pair *A* and *B* were each stimulated for 1 frame (8.3 ms); *A*/*B* interval (−8 to 8 frames) and resting period (11 to 12 frames) were blank screens (<1 cd m^{-2}). Dotted lines delineating *A* and *B* were not part of the stimuli. Average cortical firing rate during conditioning: 2.9 ± 1.5 spikes/s (SD, $n = 123$). (**C**) Responses of the neuron in (A) evoked by the stimuli in (B). (Upper) Spiking in response to *A*→*B* (red) and *B*→*A* (blue) conditioning (600 consecutive pairs each) at an 8.3-ms interval. (Lower) Post–stimulus time histograms of the responses. For this cell, the duration of the response to *A*→*B* stimuli is slightly longer than that to *B*→*A* stimuli. However, for a population of cells analyzed ($n = 90$), we found no significant difference in duration between the responses to *A*→*B* and *B*→*A* stimuli ($P > 0.40$, *t* test). (**D**) Cross-correlation between spike trains evoked by *A*→*B* and *B*→*A* stimuli. (**E**) Distribution of spike timing precision of cortical neurons, measured by the width at half height of the peak in the cross-correlogram. Arrow indicates the mean.

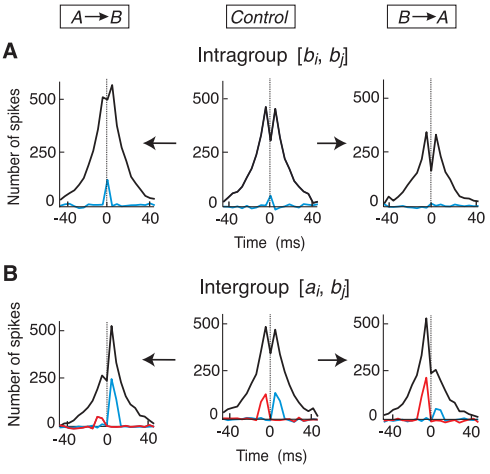

Fig. 3. Relationship between intracortical synaptic modifications and changes in cross-correlation as revealed by simulation. (**A**) Shuffle-subtracted cross-correlograms (black) between a pair of group *b* neurons (b_i and b_j) during control (middle), after *A*→*B* (left) and after *B*→*A* (right) conditioning. Blue lines, correlation due to monosynaptic common inputs from group *a* neurons to b_i and b_j (Fig. 1, A and C), obtained by eliminating all connections in the circuit except those from each group *a* neuron to b_i or b_j. (**B**) Shuffle-subtracted cross-correlograms between an intergroup pair, a_i and b_j. Red lines, correlation due to mono- and di-synaptic b_j→a_i connections, obtained by eliminating all connections except those originating from b_j and those projecting to a_i. Blue lines, correlation due to mono- and di-synaptic a_i→b_j connections.

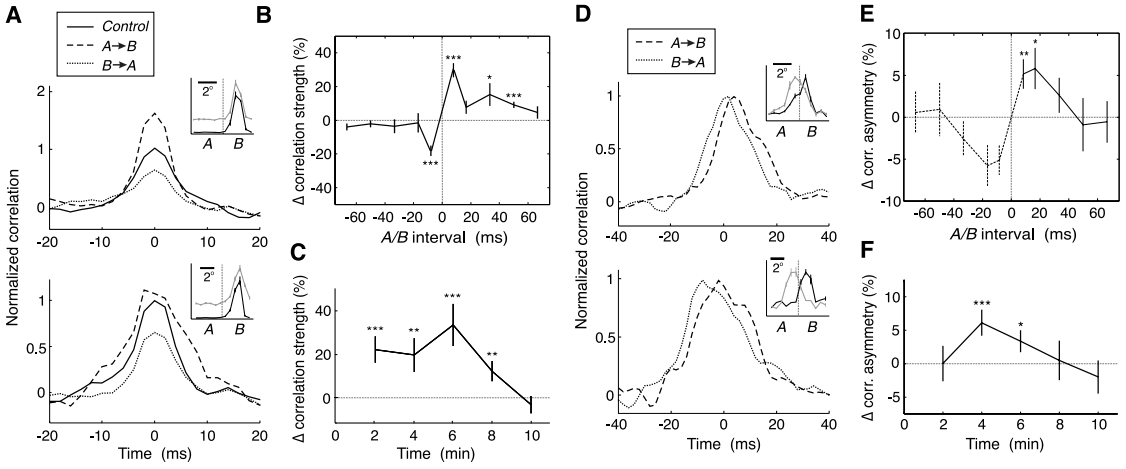

Fig. 4. Conditioning-induced changes in intracortical cross-correlation. (**A**) Two examples of changes in intragroup correlation strength. Shuffle-subtracted, flank-normalized cross-correlograms (smoothed with 1.5-ms boxcar convolution) are shown during control (solid) and after $A\rightarrow B$ (dashed) and $B\rightarrow A$ conditioning (dotted). The effects were significant for both $A\rightarrow B$ ($P < 10^{-5}$ for both examples) and $B\rightarrow A$ ($P < 0.05$ and $P < 10^{-5}$ for first and second examples, respectively) conditioning, as assessed by nonparametric bootstrap (*42*). (Insets) Receptive fields of the pair; dashed line, *A*/*B* border. The gray curve was shifted up for clarity. Error bars, ±SEM. (**B**) Changes in correlation strength as a function of *A*/*B* interval. Error bars, ±SEM ($n = 67$ to 138). Asterisks indicate data points significantly different from 0 (*$P < 0.05$; **$P < 0.01$; ***$P < 0.005$; *t* test). (**C**) Persistence of the effect ($n = 89$). Time 0 is defined as the end of conditioning. (**D**) Two examples of changes in intergroup correlation asymmetry. Cross-correlograms are shown after $A\rightarrow B$ (dashed) and $B\rightarrow A$ conditioning (dotted). The difference in asymmetry after the two types of conditioning was significant ($P < 5 \times 10^{-6}$ and $P < 0.05$ for the first and second examples, respectively). Control cross-correlogram was omitted for clarity. (**E**) Shifts in correlation asymmetry as a function of *A*/*B* interval ($n = 28$ to 58). The effects of $A\rightarrow B$ and $B\rightarrow A$ conditioning were combined as 1/2 × [asymmetry after $A\rightarrow B$ (dashed) − asymmetry after $B\rightarrow A$ (dotted)], and the left side of the curve (dashed) was plotted as the exact opposite of the right. (**F**) Persistence of the shift ($n = 34$).

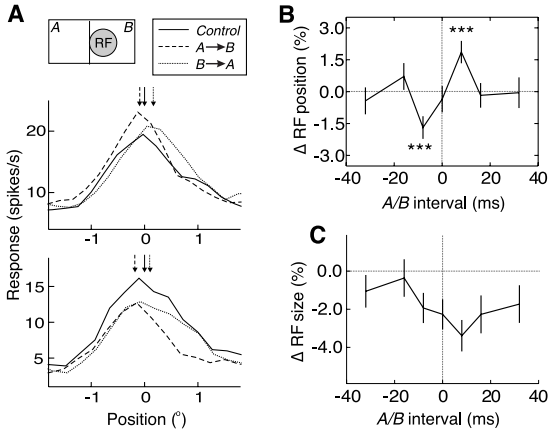

Fig. 5. Conditioning-induced shifts in cortical receptive fields. (**A**) Results from two example group *b* neurons. Receptive fields are shown during control (solid) and after $A\rightarrow B$ (dashed) and $B\rightarrow A$ (dotted) conditioning. Arrow indicates peak position of the Gaussian fit. (**B**) Normalized receptive field shift as a function of *A*/*B* interval ($n = 82$ to 154). Positive shift: toward *A*. Error bars, ±SEM. Asterisks indicate data points significantly different from 0 (***$P < 0.005$; *t* test). (**C**) Change in receptive field size as a function of *A*/*B* interval, measured from the same cells as in (B). The effects were not significantly different between $A\rightarrow B$ and $B\rightarrow A$ conditioning at each interval ($P > 0.15$, *t* test).

Cortical Receptive Fields

Conditioning-induced intracortical synaptic modifications may lead to shifts in receptive fields (Fig. 1D). We thus compared the receptive fields of each neuron mapped before and after conditioning (*17*). For both group *b* neurons shown in Fig. 5A, 800 pairs (~1.5 min) of $A\rightarrow B$ conditioning at an 8.3-ms interval induced a shift of the receptive fields toward *A*, whereas $B\rightarrow A$ conditioning induced a shift away from *A*. To quantify this effect, we fitted each receptive field with a Gaussian function and computed the difference between the peak positions of the Gaussian fits before and after conditioning (normalized by the width at half height). For the 154 group *b* neurons examined, 800 pairs of $A\rightarrow B$ conditioning (8.3-ms interval) induced a 1.86 ± 0.53% (SEM, $P < 0.001$, *t* test) shift toward *A*, whereas 800 pairs of $B\rightarrow A$ conditioning (−8.3 ms) induced a 1.69 ± 0.53% ($P < 0.002$) shift away from *A*. We further measured the effect of conditioning as a function of *A*/*B* interval from −33.3 to 33.3 ms and found significant shifts only at 8.3 and −8.3 ms (Fig. 5B), indicating temporal specificity. Thus, the direction and magnitude of shift in cortical receptive field depend on the order and interval between *A* and *B*, consistent with the prediction shown in Fig. 1D. In addition to the positions, we also compared the receptive field sizes (widths of the Gaussian fits) before and after conditioning. Conditioning induced an overall reduction of receptive field size, but the effect exhibited no systematic dependence on *A*/*B* interval (Fig. 5C).

Spatial Perception

To test whether the asynchronous conditioning can induce shift in perceptual localization (Fig. 1E), we also performed psychophysical experiments on human subjects. The conditioning stimuli were similar to those used in the physiological experiments, and a three-bar bisection test (*25*) was performed at the *A*/*B* border (Fig. 6A) to measure the perceived position of the middle bar before and after conditioning (*17*). For all four subjects tested, we found that 400 pairs (~50 s) of $A\rightarrow B$ conditioning induced a shift in the perceived location of the middle bar toward *B*, whereas $B\rightarrow A$ conditioning induced a shift toward *A*, consistent with the prediction shown in Fig. 1E. Furthermore, a significant effect was observed only at *A*/*B* intervals within ±20 ms (Fig. 6B), satisfying the temporal specificity required by the model. To further characterize the conditioning-induced perceptual shift, we measured the time course for both the induction and decay of the effect. At intervals of 8.3 ms ($A\rightarrow B$) and −8.3 ms ($B\rightarrow A$), significant shift was induced after only 100 to 200 pairs of conditioning stimuli (Fig. 6C), indicating rapid onset of the effect. After 400 pairs of conditioning stimuli, the effect showed a slight but noticeable decay over a 2-min period (Fig. 6D), suggesting that the persistence of the perceptual effect is also on the order of minutes, comparable to that observed for the intracortical synaptic modifications (Fig. 4, C and F).

Discussion

Asynchronous visual stimuli in different retinal regions induced rapid changes in cortical representation of visual space, which was likely mediated by spike timing–dependent modification of intracortical connections. Previous studies have shown that visual stimuli can induce various changes in adult cortical neurons. For example, in contrast adaptation, a few

seconds of visual stimulation in the receptive field can induce a significant reduction in the response amplitude (*26*), along with changes in receptive field size and position (*27*). These effects may be due to reduction in excitability of the cortical neurons (*28*, *29*) or homosynaptic short-term depression of the thalamic inputs (*30*). Synchronous stimulation of the receptive field center and part of the unresponsive surround can induce preferential expansion of the receptive field toward the costimulated surround region (*31*), which is likely mediated by Hebbian modification of intracortical connections. Visual conditioning with an artificial scotoma can also induce a rapid expansion of cortical receptive field inside the scotoma (*32*) and a shift in perceptual localization near the edge (*25*). The underlying mechanism is thought to be the strengthening of excitatory intracortical connections (*22*), although an alternative explanation based on contrast adaptation has also been proposed (*33*). In our study although mechanisms related to contrast adaptation may have caused the conditioning-induced reduction in receptive field size (Fig. 5C), they cannot account for the shift in receptive field position because the effect depends critically on the order and interval between stimuli in *A* and *B* (Fig. 5B). Instead, spike timing–dependent modification of intracortical connections (*1*, *3*, *5*, *6*) provides the most natural explanation. This form of synaptic plasticity is also believed to underlie conditioning-induced changes in cortical orientation tuning in both developing (*13*) and adult (*12*) animals.

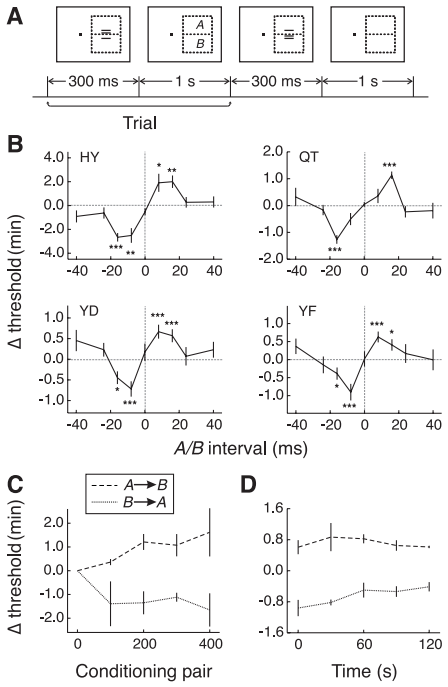

Fig. 6. Conditioning-induced shifts in human perceptual localization. (**A**) Test block with three-bar bisection task. Dotted lines delineating *A* and *B* were not part of the stimuli. (**B**) Shift in perceptual localization as a function of *A*/*B* interval for four subjects (400 conditioning pairs at each interval). Positive Δthreshold: toward *A* (shift of percept toward *B*). Error bars, ±SEM (n = 5 to 17). Asterisks indicate data points significantly different from 0 (*$P < 0.05$; **$P < 0.01$; ***$P < 0.005$; t test). YF and YD, authors; HY, experienced observer; QT, naïve subject. (**C**) Dependence of perceptual shift on the amount of conditioning at ±8.3-ms intervals. Data points represent mean shifts (±SEM) of YF, YD, and HY. The data of QT was not included because no significant effect was observed at ±8.3 ms. (**D**) Persistence of the shift induced by 400 conditioning pairs. Data points represent mean shifts of YD and YF (persistence was not measured for HY and QT).

In vitro, activity-dependent synaptic modification can last for hours (*34*, *35*). The ongoing spiking activity in vivo, however, may continuously modulate synaptic connections and obliterate the effects of conditioning over several minutes (Fig. 4, C and F). In addition, a reduction in modulatory inputs (e.g., those from the basal forebrain) caused by anesthesia may further limit the extent and persistence of conditioning-induced cortical modifications (*36*). Persistence on the order of several minutes to hours has been observed for other adult cortical modifications in vivo, including shifts in cortical receptive fields (*31*) and orientation tuning (*12*) induced by visual conditioning and modifications of intracortical connections induced by auditory conditioning (*20*). Note that the persistence of synaptic modification in the auditory cortex appears to depend on the duration of conditioning (*20*). Although ~2 min of conditioning induced a short-term modification in the visual cortex in our study, longer conditioning may cause more lasting changes.

The simple model depicted in Fig. 1 considers only spike timing–dependent modification of excitatory intracortical connections. Changes in inhibitory connections were not analyzed because they are difficult to measure with cross-correlation analysis (*19*). In the mammalian central nervous system, activity-induced modification of inhibitory synapses appears to be insensitive to the order of pre- and postsynaptic spiking (*37*), thus it may not contribute directly to the asymmetric stimulus-timing dependence of the cortical modifications observed here. Another set of excitatory connections not considered in the model are "feedforward," thalamic inputs. In principle, the asynchronous conditioning stimuli may also modify the thalamic inputs, and such modifications may cause changes in the strength of correlation between intragroup cortical cell pairs (Fig. 4, A to C) and shifts in cortical receptive fields (Fig. 5). However, modification of the thalamic inputs alone cannot account for the observed shifts in intergroup correlation asymmetry (Fig. 4, D to F), as shown by simulation studies (*38*). Thus, the cortical modifications observed in this study are likely to result at least partly from spike timing–dependent plasticity of excitatory intracortical connections. In particular, horizontal connections in layer 2/3 of the primary visual cortex play an important role in experience-dependent cortical reorganization during development (*39*), and spike timing–dependent modification of these connections is a robust phenomenon in vitro (*6*).

Spike timing on the order of 10s of milliseconds plays an important role in both coding of visual information (*40*, *41*) and modification of neuronal circuitry (*1*–*6*). We found that spiking of the cortical neurons was time-locked to the flashed visual stimuli with a precision of ~30 ms (Fig. 2, C to E), allowing timing of visual stimuli on the order of 10s of milliseconds to be represented by spike timing in the cortical circuit. The marked dependence of cortical modifications on stimulus timing, observed at the levels of intracortical synaptic connectivity, receptive field properties, and human visual perception, attests to the critical role of stimulus timing in activity-dependent plasticity of adult visual cortex.

References and Notes

1. H. Markram, J. Lubke, M. Frotscher, B. Sakmann, *Science* **275**, 213 (1997).
2. L. I. Zhang, H. W. Tao, C. E. Holt, W. A. Harris, M. Poo, *Nature* **395**, 37 (1998).
3. D. E. Feldman, *Neuron* **27**, 45 (2000).
4. C. A. Boettiger, A. J. Doupe, *Neuron* **31**, 809 (2001).
5. P. J. Sjostrom, G. G. Turrigiano, S. B. Nelson, *Neuron* **32**, 1149 (2001).
6. R. C. Froemke, Y. Dan, *Nature* **416**, 433 (2002).
7. L. F. Abbott, K. I. Blum, *Cereb. Cortex* **6**, 406 (1996).
8. W. Gerstner, R. Kempter, J. L. van Hemmen, H. Wagner, *Nature* **383**, 76 (1996).
9. S. Song, K. D. Miller, L. F. Abbott, *Nature Neurosci.* **3**, 919 (2000).
10. R. P. N. Rao, T. J. Sejnowski, in *Advances in Neural Information Processing Systems*, S. A. Solla, T. K. Leen, K. R. Muller, Eds. (MIT Press, Cambridge, MA, 2000).
11. M. R. Mehta, M. C. Quirk, M. A. Wilson, *Neuron* **25**, 707 (2000).
12. H. Yao, Y. Dan, *Neuron* **32**, 315 (2001).
13. S. Schuett, T. Bonhoeffer, M. Hubener, *Neuron* **32**, 325 (2001).
14. C. D. Gilbert, *Physiol. Rev.* **78**, 467 (1998).
15. Potentiation of $a \rightarrow b$ connections enhances the responses of group *b* neurons to visual stimuli in *A*, causing group *b* receptive fields to shift toward *A*; depression of $b \rightarrow a$ connections reduces the responses of group *a* neurons to stimuli in *B*, causing group *a* receptive fields to shift away from *B*. Thus, synaptic modifications induced by $A \rightarrow B$ conditioning cause the receptive fields of both groups to shift toward *A*. Such shifts have been confirmed by simulation studies (*17*).
16. S. Deneve, P. E. Latham, A. Pouget, *Nature Neurosci.* **2**, 740 (1999).
17. Materials and Methods are available as supporting material on *Science* Online.
18. D. H. Perkel, G. L. Gerstein, G. P. Moore, *Biophys. J.* **7**, 419 (1967).
19. A. M. Aertsen, G. L. Gerstein, *Brain Res.* **340**, 341 (1985).
20. E. Ahissar, *et al.*, *Science* **257**, 1412 (1992).

21. R. C. Reid, J. M. Alonso, *Nature* **378**, 281 (1995).
22. A. Das, C. D. Gilbert, *J. Neurophysiol.* **74**, 779 (1995).
23. J. M. Alonso, L. M. Martinez, *Nature Neurosci.* **1**, 395 (1998).
24. Correlation asymmetry is defined as $(R - L)/(R + L)$, where R is the area of the right side of the peak in the cross-correlogram and L is the area of the left side (*23*).
25. M. K. Kapadia, C. D. Gilbert, G. Westheimer, *J. Neurosci.* **14**, 451 (1994).
26. L. Maffei, A. Fiorentini, S. Bisti, *Science* **182**, 1036 (1973).
27. S. Marlin, R. Douglas, M. Cynader, *J. Neurophysiol.* **69**, 2209 (1993).
28. M. Carandini, D. Ferster, *Science* **276**, 949 (1997).
29. M. V. Sanchez-Vives, L. G. Nowak, D. A. McCormick, *J. Neurosci.* **20**, 4267 (2000).
30. F. S. Chance, S. B. Nelson, L. F. Abbott, *J. Neurosci.* **18**, 4785 (1998).
31. U. T. Eysel, D. Eyding, G. Schweigart, *NeuroReport* **9**, 949 (1998).
32. M. W. Pettet, C. D. Gilbert, *Proc. Natl. Acad. Sci. U.S.A.* **89**, 8366 (1992).
33. G. C. DeAngelis, A. Anzai, I. Ohzawa, R. D. Freeman, *Proc. Natl. Acad. Sci. U.S.A.* **92**, 9682 (1995).
34. R. A. Nicoll, R. C. Malenka, *Nature* **377**, 115 (1995).
35. D. J. Linden, J. A. Connor, *Annu. Rev. Neurosci.* **18**, 319 (1995).
36. J. M. Edeline, *Prog. Neurobiol.* **57**, 165 (1999).
37. L. F. Abbott, S. B. Nelson, *Nature Neurosci.* **3**(suppl.), 1178 (2000).
38. Y.-X. Fu *et al.*, unpublished data.
39. J. T. Trachtenberg, C. Trepel, M. P. Stryker, *Science* **287**, 2029 (2000).
40. W. Singer, C. M. Gray, *Annu. Rev. Neurosci.* **18**, 555 (1995).
41. W. Bair, *Curr. Opin. Neurobiol.* **9**, 447 (1999).
42. B. Efron, R. J. Tibshirani, *An Introduction to the Bootstrap* (Chapman and Hall, New York, 1993).
43. This work was supported by grants from the Whitaker Foundation, the National Science Foundation, and the National Eye Institute. We thank the University of Michigan for kindly providing the multielectrodes.

Supporting Online Material
www.sciencemag.org/cgi/content/full/296/5575/1999/DC1
Materials and Methods

4 February 2002; accepted 6 May 2002

Submicrometer Ferromagnetic NOT Gate and Shift Register

D. A. Allwood, Gang Xiong, M. D. Cooke, C. C. Faulkner, D. Atkinson, N. Vernier, R. P. Cowburn*

An all-metallic submicrometer device is demonstrated experimentally at room temperature that performs logical NOT operations on magnetic logic signals. When this two-terminal ferromagnetic structure is incorporated into a magnetic feedback loop, the junction performs a frequency division operation on an applied oscillating magnetic field. Up to 11 of these junctions are then directly linked together to create a magnetic shift register.

Devices for information technology have generally been dominated by electronics. However, emerging spin-electronics, or "spintronic," technologies (*1*, *2*), which are based on electron spin as well as charge, may offer new types of devices that outstrip the performance of traditional electronics devices. Spintronic devices use magnetic moment to carry information; advantages of such devices often include low power dissipation, nonvolatile data retention, radiation hardness, and high integration densities. Although the future of spintronics might include a solid-state realization of quantum computing (*3*), the experimental observations to date of optically (*4*) and electrically (*5*) controlled magnetism, spin-polarized current injection into semiconductors (*6*–*8*), ferromagnetic imprinting of nuclear spins (*9*), and control of electron-nuclei spin interactions (*10*) suggest a whole range of spintronic applications. Already, spintronic hard disk drive read-heads are well established commercially, and magnetic random access memories (MRAM) look set to follow suit.

To date, two classes of spintronic device have been proposed: semiconductor and metallic. Semiconductor devices will use spin population imbalances between electrons or nuclei. Metallic devices, including hard disk read-heads and MRAM, represent information by the magnetization direction in a ferromagnetic metal such as NiFe (Permalloy) or Co. Much work has focused on writing information to this ferromagnetic element, for example, using magnetic fields from current-carrying wires and reading information using either giant magnetoresistance (*11*) or spin-dependent tunneling junctions (*12*). However, the extent to which information can be manipulated in the magnetic form has, to date, been very limited; MRAM cells, for instance, can only store information. The scope of spintronics could be greatly expanded if in addition to data storage, magnetic data bits could interact to perform some computation between being written and detected. Magnetic information has been propagated along chains of 100-nm-diameter magnetic dots (*13*) to allow signal interconnection. However, a full logic scheme will require the development of magnetic structures that perform basic logic operations, including NOT gates for inversion operations. Such structures will form the building blocks of magnetic logic devices that perform operations analogous to current microelectronics.

Under low–magnetic field conditions, the magnetization direction within submicrometer ferromagnetic planar wires tends to lie along the wire long-axis owing to strong magnetic shape anisotropy. When two oppositely directed magnetizations meet within a wire, the realignment of successive atomic magnetic moments is not abrupt but occurs gradually over a certain distance to form a domain wall. For the 200-nm-wide, 5-nm-thick Permalloy ($Ni_{80}Fe_{20}$) wires investigated here, we calculate, using micromagnetic software (OOMMF) (*14*), that domain walls should be ~100 nm wide. It is now known that domain walls can propagate along straight submicrometer magnetic wires by application of a magnetic field parallel to the wire (*15*). A magnetic field with a vector that rotates with time in the sample plane can be used to propagate domain walls along magnetic wires that change direction and turn corners. The clockwise or counterclockwise rotation defines the magnetic field chirality, or handedness. A domain wall should propagate around a magnetic wire corner providing that the field and corner are of the same chirality. However, the chirality of a corner depends on the direction of domain wall propagation so that, within a rotating magnetic field of given chirality, a domain wall will only be able to pass through a given corner in one direction. This applies for domain walls with adjacent magnetizations either converging or diverging and satisfies the important requirement of any logic system that a definite signal flow direction must exist.

The two stable magnetization directions within submicrometer magnetic wires provide a natural means of representing the two Boolean logic states, 1 and 0. However, if there is a 180° bend in a magnetic wire and magnetization is continuous throughout, the absolute direction of magnetization will be different before and after the bend. Care must be taken in assigning logical states to different magnetization directions to avoid confusion in such situations. Therefore, we assign logical 1 to wire magnetization being in the same direction as domain wall motion and logical 0 to the magnetization direction opposing domain wall motion. Using this defi-

Department of Physics, University of Durham, Rochester Building, Science Laboratories, South Road, Durham DH1 3LE, UK.

*To whom correspondence should be addressed. E-mail: r.p.cowburn@durham.ac.uk